Research on Chemical Intermediates (2020) 46:4383–4402
https://doi.org/10.1007/s11164-020-04210-y

Methane activation on PdMn/C-ITO electrocatalysts using a reactor-type PEMFC

J. Nandenha[1] · J. Y. Yamashita[1] · F. M. Souza[2] · E. H. Fontes[1] · B. L. Batista[2] · M. C. Santos[2] · M. Linardi[1] · A. O. Neto[1]

Received: 2 March 2020 / Accepted: 6 July 2020 / Published online: 17 July 2020

Abstract

Various palladium and manganese supported in a mix of carbon and indium thin oxide (PdMn/C-ITO) compositions were synthesized by a sodium borohydride reduction process for methane activation at low temperatures in a proton exchange membrane fuel cell (PEMFC) reactor. These electrocatalysts were characterized by X-ray diffraction, transmission electron microscopy (TEM), X-ray photoelectron spectroscopy XPS, inductively coupled plasma mass spectrometry ICP-MS, attenuated total reflection-Fourier transform infrared spectroscopy, cyclic voltammetry and a PEMFC reactor. The diffractograms of PdMn/C-ITO electrocatalysts revealed the face-centered cubic structure of palladium and the bixbyite cubic structure of In_2O_3. TEM experiments showed mean nanoparticle sizes between 4.7 and 5.2 nm for all electrocatalysts. XPS results showed the presence of palladium and manganese oxides, as well as Pd^0 species. Cyclic voltammograms of PdMn/C-ITO electrocatalysts showed an increase in current density values after the methane adsorption, this result is related to formation of methanol or formic acidic. Polarization curves at 80 °C acquired in a PEMFC reactor showed that PdMn(70:30)/C-ITO and PdMn(50:50)/C-ITO have superior performance when compared to Pd/C-ITO indicating the beneficial effect of adding Mn, this behavior can be attributed to the bifunctional mechanism or to the electronic effect of support.

Keywords Sodium borohydride reduction process · PdMn/C-ITO electrocatalysts · Methane oxidation · PEMFC reactor · ATR-FTIR studies

✉ A. O. Neto
aolivei@ipen.br; neto.almir@bol.com.br

[1] Energy and Nuclear Research Institute, IPEN/CNEN-SP, Av. Prof. Lineu Prestes, 2242 Cidade Universitária, São Paulo, SP CEP 05508-000, Brazil

[2] Natural and Human Sciences Center, Federal University of ABC, Rua Santa Adélia, 166, Santo André, SP 09210-170, Brazil

Introduction

The use of natural gas for power generation is very interesting nowadays due to its abundance on planet earth. Furthermore, methane is considered the main component of natural gas [1–4]. This type of gas is used for heating, cooking, transportation purposes and electricity generation [3]. The methane shows low electron and proton affinity, low polarizability, weak acidity, high C–H bond energy (439 kJ mol^{-1}) and high ionization energy, and it is very inert [5, 6], so methane oxidation is a considerable challenge. Methane can also increase the global warming if it is converted to carbon dioxide. But if we use for other purposes, since oil fields hasn't enough infrastructure to store and transport gaseous methane and apply them for a specific use. The solution might be to oxidize methane to sub-products of oxidation, for instance, methanol. These studies could be realized in a reactor-type fuel cell as described in [7–11].

Polymeric electrolyte membrane fuel cell (PEMFC) is a type of fuel cell constituted of two electrodes (anode and cathode) separated by a Nafion® electrolyte [13]. PEMFC is used as an alternative source of energy for automobile, laptop computers, cell phones and other electronic devices that requires low operating temperature, possesses high power density and is usually light weight [12, 13].

Palladium electrocatalysts are commonly used for the methane combustion [14]. Normally, Pd electrocatalysts have a low stability for methane combustion when the temperature is kept constant, and their, initially, high activity drops significantly during operation, especially for pure electrocatalysts [14, 15]. In addition, methane combustion over Pd-based electrocatalysts is strongly inhibited by water vapor, which is present at 5–10% in engine exhaust gas [15].

Willis et al. [16] reported the use of colloidal bimetallic nanocrystals to produce Pd-Metal electrocatalysts to methane oxidation. These authors showed a single synthetic protocol to obtain uniform palladium-based bimetallic nanocrystals (PdM, M = V, Mn, Fe, Co, Ni, Zn and Sn) with a wide variety of compositions and sizes based on high-temperature thermal decomposition of readily available precursors. They concluded that some metals as Fe, Co and Sn inhibit the sintering of the active Pd phase, while other metals as Mn, Ni and Zn increased the activity compared to Pd electrocatalyst.

Xu et al. [17] prepared a PdMn/RGO electrocatalysts by sodium borohydride reduction and tested these materials for methanol oxidation in alkaline conditions. PdMn/RGO showed a better catalytic activity than Pd/RGO for methanol oxidation, where this behavior was attributed to the better dispersion of nanoparticles on the surface of RGO.

Matin et al. [18] prepared a PdMn/C by sonochemical reactions for formic acidic oxidation, these authors observed that the incorporation of Mn in Pd reduced the poisoning of surface by hydroxyl groups and PdMn/C improved durability in comparison with Pd/C.

Ahmed et al. [19] prepared PdMn/G with various ratios atomic for ethanol oxidation in this work was observed a superior catalytic activity and stability for

PdMn/G (50:50) in comparison with Pd/G, this behavior was assigned to the degree of alloying.

Carbon is the most common and preferred catalyst support material for (PEMFCs) and alkaline fuel cells (AFCs), because it is abundant, it has a high surface area and good electrical conductivity, however, the use of carbon is problematic due to its low resistance to corrosion [20]. The nature of carbon-based supports is critical for the activity, dispersion, stability, mass transfer kinetics at the electrode surface and electric conductivity of an electrocatalyst [21, 22]. An alternative to the carbon support it is the use of metal oxides, because they can be easily prepared in the desired sizes and shapes, and are non-toxic [20, 23]. Tin-doped indium oxide ($In_2O_3{\cdot}SnO_2$, also called ITO) is one of the materials used as support that has received increasing interest due to its low cost and prominent characteristics which include: high electrical conductivity, and excellent optical transparency [24]. Tin-doped indium oxide (ITO) have some suitable properties with respect to durability issues in PEMFCs like the already oxidized stage [25] and the almost stable characteristics in strong acidic environments and enhanced temperatures [25, 26].

Mustain et al. [27] synthesized and investigated Tin-doped indium oxide as the supports for Pt electrocatalysts. The electrochemical stability of the platinized and oxide supports was examined from − 0.8 to 1.4 V versus NHE. These authors observed that the Tin-doped indium oxide surface was generally stable at positive potentials, but experienced severe degradation at negative potentials due to the reduction/oxidation of the surface.

Liu et al. [23] indicated that oxide supports were also able to affect the activity of the supported noble metals due to metal-support interactions. These interactions including a modification of the electronic states of Fermi level of Pt that pushes the formation of Pt–OH groups to higher potentials [27]; spillover of OH groups onto the oxide support; and OH reduction coverage by lateral repulsion between Pt–OH and oxide surfaces [28].

In this context, the aim of this work was to synthesize Pd/C-ITO, Mn/C-ITO and various PdMn/C-ITO by first time using the sodium borohydride reduction method, and to test them for methane activation in acid medium. This work correlates surface and structural characterizations, electrochemical experiments and PEMFC reactor experiments.

Experimental

Synthesis of the Pd/C-ITO, Mn/C-ITO and PdMn/C-ITO electrocatalysts

PdMn/C-ITO electrocatalysts with atomic ratios of 90:10, 70:30 and 50:50, and 20% of metal loading, were prepared using $Pd(NO_3)_2{\cdot}2H_2O$ (Aldrich) and $MnCl_2{\cdot}4H_2O$ (Synth) as metal sources and sodium borohydride ($NaBH_4$, Aldrich) as reducing agent. A physical mixture of 85% Vulcan Carbon XC72 (Cabot) + 15% ITO ($In_2O_3{\cdot}SnO_2$ nanopower < 50 nm particle size, 85–90 wt% and 10–15 wt% SnO_2 Aldrich) was used as support. The choice of the respective binary compositions was based on Pereira et al. and De Camargo et al. works [29, 30]. The mixture of 85%

Vulcan Carbon XC72 + 15% ITO was dispersed into a solution of water/2-propanol (50/50, v/v), containing metal ions of Pd or Pd and Mn. The solution resulting was submitted to an Ultrasonic Probe Sonicator by 10 min for homogenization. After the $NaBH_4$ solution in 0.01 mol L^{-1} NaOH was added. The resulting solution was maintained under stirring for an additional 1 h at room temperature for reduction of metals. Finally, the material was filtered and washed with high-purity deionized water and dried in a Thermostatic Laboratory Stove at 70 °C for 2 h [10, 31]. The material was macerated and a fine powder was obtained, and its mass was weighed on a semi-analytical balance to check the metal load present.

X-ray diffraction (XRD) and transmission electron microscopy (TEM)

PdMn/C-ITO electrocatalysts were characterized by X-ray diffraction analysis using CuKα radiation source ($\lambda = 0.15406$ nm), where the diffractograms were recorded in the range of $2\theta = 20°$ to 90° with a step size of 0.05° and a scan time of 2 s per step [32, 33]. The morphology, size and nanoparticle distribution of PdMn/C-ITO electrocatalysts were determined by transmission electron microscopy using a JEOL electron microscope model JEM-2100 operated at 200 kV. For the construction of the histograms and determination of mean, nanoparticle sizes were measured over 170 nanoparticles from nine micrographs [10].

Elemental composition by ICP-MS analysis

The elementary compositions of the PdMn/C-ITO electrocatalysts were determined using an inductively coupled plasma mass spectrometer (ICP-MS, Agilent 7900, Hachioji, Japan) operated with high-purity argon (99.9999%, White Martins, Brazil). All reagents were of analytical grade. HNO_3 and HCl were purified by using a Teflon sub-boiling distiller (DST-100, Savillex, USA). High-purity deionized water (resistivity 18.2 MΩ cm) was generated with a Milli-Q water purification system (Millipore, Bedford, MA, USA) [34]. The Pd and Mn extraction was carried out using a closed vessel system. Approximately 20 mg of electrocatalyst was placed into 50 mL test tubes that contained 3 mL of HNO_3 + 1 mL of HCl, and the test tubes were then closed. Then, the test tubes stood for 24 h at 25 °C. Finally, the volume was increased to 50 mL, and the elemental composition was determined by ICP-MS [34]. The isotopes monitored were ^{105}Pd, ^{55}Mn during analysis was used ^{89}Y (25 μg L^{-1}) as internal standard and the calibration curve ranged from 1 to 50 μg L^{-1} for Pd, Mn, In and Sn ($R^2 = 0.9999$).

X-ray photoelectron spectroscopy (XPS)

X-ray photoelectron spectroscopy (XPS) measurements of PdMn/C-ITO electrocatalysts were carried out by a Thermo Scientific K-Alpha$^+$, spectrometer a monochromated with AlKα X-ray source radiation ($h\upsilon = 1486.6$ eV) and a spot diameter of 400 μm at base pressure below of 5×10^{-7} Pa. Binding energies were referenced against the main C(1s) line of adventitious carbon impurities at 284.6 eV. Peak

energies were given to an accuracy of 0.1 eV. The spectra were deconvoluted and optimized using a Levenberg–Marquardt Algorithm with U2 Tougaard background in the Casa XPS software.

Cyclic voltammetry (CV)

The cyclic voltammetry of the PdMn/C-ITO electrocatalysts were carried out with an AutoLab PGSTAT30 Potentiostat/Galvanostat with GPES Software coupled to the interface, at ambient temperature in a 0.5 mol L^{-1} $HClO_4$ solution using a three electrodes conventional glass cell. The reversible hydrogen electrode (RHE) was used as a reference electrode, a Pt wire as a counter electrode and the thin porous carbon coating technique as working electrode with a geometrical surface area of 0.5 cm^2 with a depth of 0.3 mm as previously reported [35]. Our RHE consists of a platinum wire in a glass compartment, where hydrogen gas is generated by applying a voltage by the potentiostat. The electrocatalyst suspension was then compressed wet yet onto the glassy carbon electrode in a nitrogen gas stream. The cyclic voltammetry experiments were done at a scan rate of 10 mV s^{-1} for the potential range from 0.05 to 1.2 V versus RHE with the presence or absence of methane [36]. The methane adsorption was realized at 0.5 V versus RHE with bubbling for 1800 s in 0.5 mol L^{-1} $HClO_4$, using a rotating disk electrode setup. For the oxygen reduction reaction (ORR) electrochemical measurements, the same setup of cyclic voltammetry was maintained. The ORR measurements were done with oxygen purged [35], and with oxygen and methane both purged for 1800 s in 0.5 mol L^{-1} $HClO_4$ at a scan rate of 10 mV s^{-1} for the potential range from 1.2 to 0.05 V versus RHE.

Attenuated total reflection-Fourier transform infrared (ATR-FTIR)

The ATR-FTIR measurements for PdMn/C-ITO electrocatalysts were performed on a spectrometer equipped with an MCT detector cooled with liquid N_2. The ATR accessory with internal reflection element Diamond/ZnSe is coupled to the spectrometer [36, 37], where an electrochemical cell is connected above the internal reflection element. The working electrode was an ultrathin porous carbon coating technique in the presence of 0.5 mol L^{-1} $HClO_4$ saturated with CH_4 gas for 1800 s. The background spectra were collected following Nandenha et al. works [10].

Fuel cell experiment

For experiments in fuel cell, the Membrane Electrode Assemblies (MEAs) were prepared by hot pressing at 125 °C for 5 min under pressure of 225 kgf cm^{-2} using a pretreated Nafion® 117 membranes placed between anode (PdMnC-ITO), and cathode (Pt/C BASF) electrocatalysts. The PdMnC-ITO electrodes and the cathode prepared in this work were made with 1 $mg_{(Pd)}$ cm^{-2} electrocatalyst loading [38]. The methane studies in the PEMFC were made in a typical single fuel cell modified (reactor methane proton exchange membrane fuel cell—DMPEMFC) with an area of 5 cm^2. The temperatures were set to 80 °C for the fuel cell and 85 °C for the

Table 1 Nominal and real (EDS) mass ratios of the PdMn/C-ITO binary electrocatalysts

Electrocatalysts	Nominal mass ratios (%) (Pd:Mn)	Real mass ratios: EDS (%) (Pd:Mn)
PdMn/C-ITO	90:10	89.45:10.55
PdMn/C-ITO	70:30	73.54:26.46
PdMn/C-ITO	50:50	53.81:46.19

Table 2 Concentration of metals to electrocatalysts from ICP-MS experiment

Electrocatalysts	Pd	Mn	In	Sn
Pd/C-ITO	20.3 ± 0.3	n.d.†	10.1 ± 0.2	0.8 ± 0.1
Mn/C-ITO	n.d.†	20.5 ± 0.3	9.1 ± 0.1	0.7 ± 0.2
PdMn(90:10)/C-ITO	20.5 ± 0.3	1.4 ± 0.1	11.5 ± 0.1	0.9 ± 0.1
PdMn(70:30)/C-ITO	15.8 ± 0.2	3.7. ± 0.1	10.0 ± 0.2	0.8 ± 0.1
PdMn(50:50)/C-ITO	13.8 ± 0.2	7.1 ± 0.1	10.3 ± 0.1	0.9 ± 0.1

†n.d. = Not determined

methane humidifier and 85 °C for the oxygen humidifier. The fuel was 500 mL of 99% methane gas at approximately 150 mL min^{-1}, the oxygen flow was regulated at 200 mL min^{-1} and pressure atmospheric was also set [36]. Polarization curves were obtained using an AutoLab PGSTAT302N Potentiostat/Galvanostat with GPES Software coupled, which receives the electric current produced by it, and connected in the fuel cell.

Results and discussion

EDS analysis

The EDS analysis of PdMn(90:10)/C-ITO, PdMn(70:30)/C-ITO and PdMn(50:50)/C-ITO are shown in Table 1. The EDS analysis of these electrocatalysts has good correlation between the nominal mass ratios and the real mass ratios. This indicates the efficiency of the synthesis to prepare the PdMn/C electrocatalysts.

ICP-MS analysis

The concentrations of the analyzer metals by ICP-MS are shown in Table 2. The concentration of Pd and Mn was satisfactory in the electrocatalysts because they are close to what was expected. The concentration of Pd in the electrocatalysts, obtained by ICP-MS, was used to normalize the results of the electrocatalytic activity. The In and Sn concentration results showed that the mass ratio of In:Sn is approximately 10:1, respectively. In addition, the concentration of ITO (In:Sn oxide) is within the expected.

XRD analysis

Figure 1 shows the X-ray diffractograms of Pd/C-ITO, Mn/C-ITO, PdMn(90:10)/C-ITO, PdMn(70:30)/C-ITO and PdMn(50:50)/C-ITO electrocatalysts prepared by sodium borohydride reduction. For all electrocatalysts, synthesized were observed a broad peak at about $2\theta \approx 25°$ associated to the Vulcan Carbon XC72 support material. The X-ray diffractograms of Pd/C-ITO, and PdMn/C-ITO electrocatalysts in this work presented four peaks at about $2\theta = 40°$, 46°, 68°, and 82°, which are associated with the crystal planes (111), (200), (220), and (311), corresponding to the face-centered cubic structure (fcc) of palladium (JCPDS46-1043) and its alloys [10, 36, 39]. The X-ray diffractograms for all electrocatalysts also showed peaks at about $2\theta = 20°$, 31°, 35°, 46°, 51°, 61° and 83°, which are associated with the crystal planes (211), (222), (400), (134), (440), (622) and (662), associated with the presence of a bixbyite In_2O_3 cubic structure (JCPDS 65-3170) with no secondary phases, indicating the effective incorporation of Sn into the In_2O_3 [21, 26]. For Mn/C-ITO, and PdMn/C-ITO electrocatalysts, no peaks relative to Mn or its oxides were detected; nevertheless, the presence of these peaks cannot be dismissed since pure Mn or its oxides can be present in an amorphous form [40].

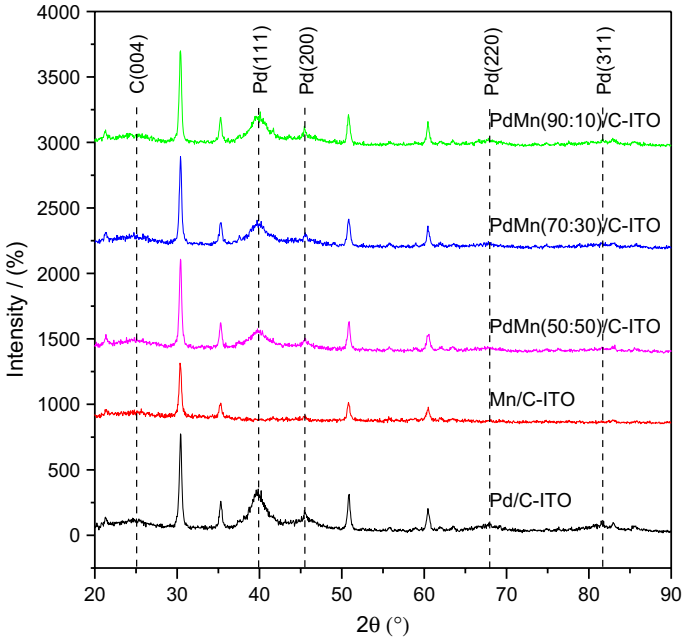

Fig. 1 XRD patterns obtained from Pd/C-ITO, Mn/C-ITO, PdMn(90:10)/C-ITO, PdMn(70:30)/C-ITO, and PdMn(50:50)/C-ITO electrocatalysts, prepared by the sodium borohydride method

TEM analysis

The TEM images of different electrocatalysts are shown in Fig. 2. The average size of Pd was 5.22 nm for Pd/C, 5.08 nm for PdMn(90:10)/C-ITO, 5.04 nm for PdMn(70:30)/C-ITO and 4.73 nm for PdMn(90:10)/C-ITO, respectively, and of Mn was 4.60 nm for Mn/C-ITO, grown on the carbon plus ITO surface. The metal particles of all electrocatalysts synthesized were uniformly deposited on the support (C-ITO), with formation of some agglomerates [41, 42]. The agglomeration phenomenon could be explained by the presence of ITO ($In_2O_3{\cdot}SnO_2$) mixed with carbon used as support, and by a fast reduction process [18, 43]. The insertion of Mn content in Pd/C-ITO electrocatalysts decreased the mean particle diameter. This decrease is due to the little electrocatalyst sintering, and due to the presence of the second metal Mn in the whole particle incorporated into the lattice structure, confirmed by XRD. Furthermore, Mn/C-ITO electrocatalyst showed the smallest size while Pd/C-ITO presented the largest one (Fig. 2).

XPS analysis

Elemental analysis indicated that the ratio of Pd and Mn is close to that expected are shown in Table 3. It is important to notice that the atomic composition obtained from survey XPS has different correlations when compared to the EDS analysis, because the different metal oxidation states can be convoluted with the M^0 in the nl_j states, where M^0 is the null oxidation state metal.

Figure 3 shows the core-level XPS spectra of the electrocatalysts indicating the presence of the elements. C1s peak revealed the presence of C–C bond characteristic and predominant in Carbon Vulcan XC72 support [38] as well as the shake up peak. Sn3d doublet showed only the presence of the SnO_2 species, which is consistent with the XRD results.

In3d doublet presented two different oxidation states In_2O and In_2O_3 (Fig. 4). O1s band showed the indirect presence of the $Pd3p_{3/2}$ state as well as the O1s prevenient from the external environment and C–O–C which is probably due to the interaction between oxygen atoms and the Carbon Vulcan XC72 support [38].

Pd3d doublet showed the presence of Pd^0 state as well as the PdO oxidation state, while Mn2p revealed the presence of only MnO species (Fig. 5). All these oxidation states and its respective binding energies are in accordance with Ref. [44].

We strongly believe that the different oxidation states are correlated with the metal salts reducing agent used, which is in our case the sodium borohydride. In the work of [38], they found similar oxidation states using this same reducing agent. Besides the use of the reducing agent, the electrocatalysts surfaces are exposed and interacting with the oxygen from the air which inevitable lead to the formation of metal oxides.

Electrochemical experiments

Cyclic voltammograms results for PdMn/C-ITO electrodes were recorded in a pure electrolyte solution 0.5 mol L^{-1} $HClO_4$ and 0.5 mol L^{-1} $HClO_4 + CH_4$ at room temperature with sweep rates from 10 mV s^{-1} (Fig. 4). The adsorption–desorption

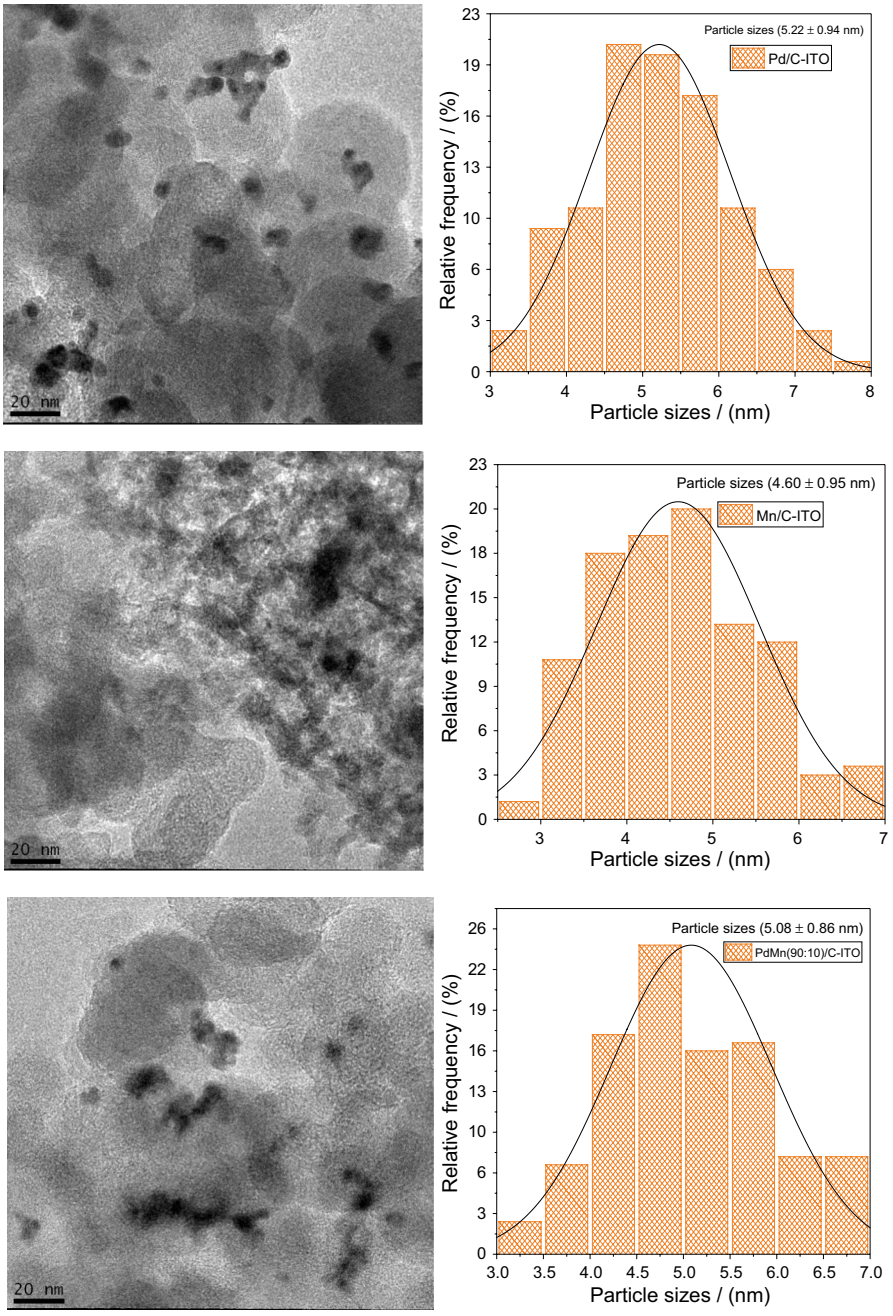

Fig. 2 TEM images and histograms of the nanoparticles size distribution to Pd/C-ITO, Mn/C-ITO, PdMn(90:10)/C-ITO, PdMn(70:30)/C-ITO and PdMn(50:50)/C-ITO electrocatalysts

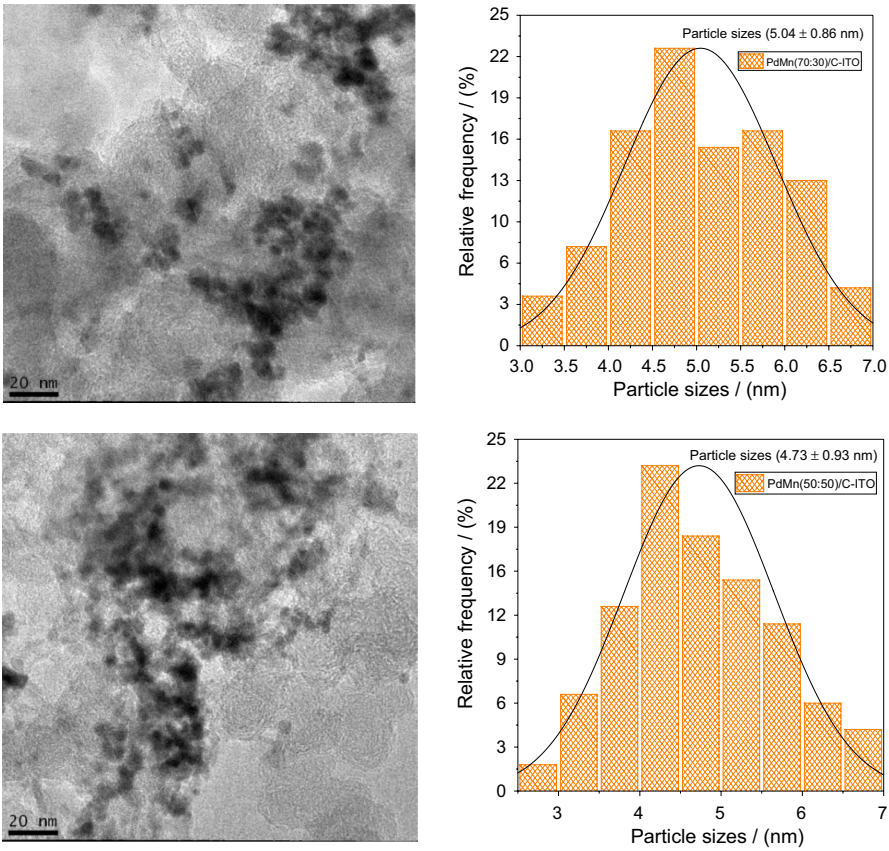

Fig. 2 (continued)

Table 3 Metal concentration of electrocatalysts obtained from survey XPS analyses

Electrocatalyst	Pd:Mn (% atomic)		In:Sn (% atomic)	
	Pd	Mn	In	Sn
Pd/C-ITO	13.9 ± 1.5‡	n.d.†	70.4 ± 9.9	29.6 ± 9.9
Mn/C-ITO	n.d.†	22.6 ± 1.4‡	62.7 ± 10.9	37.3 ± 10.9
PdMn(90:10)/C-ITO	77.4 ± 5.1	22.6 ± 5.1	76.6 ± 7.4	23.4 ± 7.4
PdMn(70:30)/C-ITO	53.2 ± 4.8	46.8 ± 4.8	78.3 ± 6.1	21.7 ± 6.1
PdMn(50:50)/C-ITO	45.2 ± 4.9	54.8 ± 4.9	81.5 ± 12.5	18.5 ± 12.5

†n.d. = not determined

‡Compared with carbon

region on Pd in the 0.5 mol L^{-1} $HClO_4$ electrolyte (solid line), and after methane adsorption (color lines) at 0.05 V while bubbling methane for 30 min in 0.5 mol L^{-1} $HClO_4$, occurring between 0.05 and 0.50 V versus RHE [10, 45].

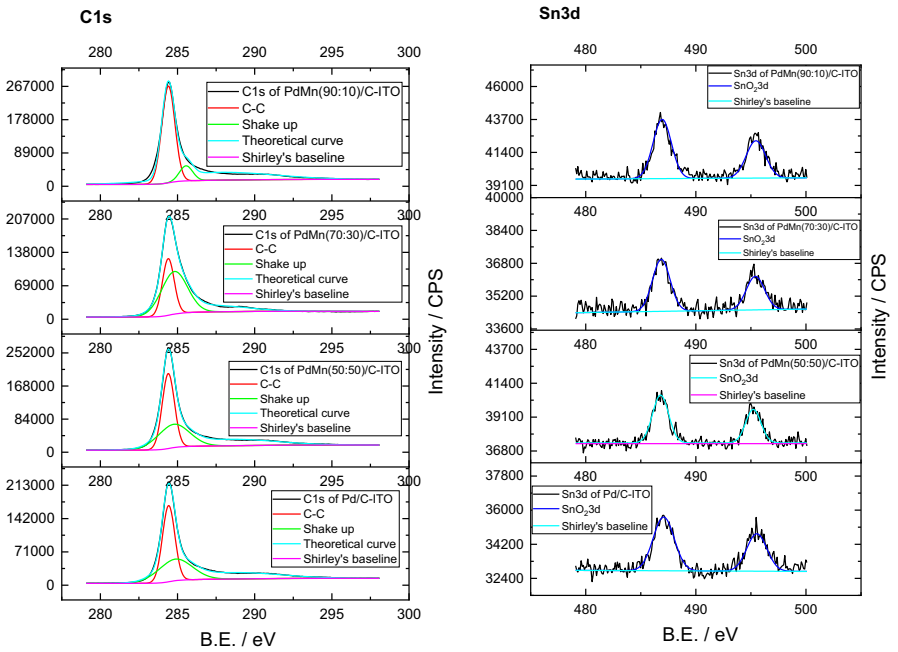

Fig. 3 Core-level XPS spectra of C1s and Sn3d of Pd/C-ITO, PdMn(90:10)/C-ITO, PdMn(70:30)/C-ITO and PdMn(50:50)/C-ITO electrocatalysts

For all synthesized electrocatalysts (solid line), it is observed that the hydrogen adsorption–desorption regions increase partially in comparison with cyclic voltammograms before methane adsorption. This indicates the presence of oxidized species covering the electrode surface. Also, was observed an increase in current during the anodic scan which corresponds to the adsorbed species oxidation [10]. The Mn/C-ITO exhibited a low hydrogen adsorption charge, compared to Pd/C-ITO and all PdMn/C-ITO electrocatalysts, which could be attributed to the hydrogen adsorption (H_{ads}) and absorption properties of Mn (solid line). PdMn(50:50)/C-ITO electrocatalyst indicated large hydrogen adsorption charges, while the Pd/C and PdMn(90:10)/C-ITO electrocatalysts showed similar hydrogen adsorption charges. The double layer (0.30 V and 0.75 V vs. RHE) was similar for the PdMn(70:30)/C-ITO and PdMn(50:50)/C-ITO electrocatalysts, and in the oxides (PdO) region (0.70 V and 1.2 V vs. RHE). However, PdMn(50:50)/C-ITO presented a higher current density compared to the others electrocatalysts. The Pd/C-ITO electrocatalyst showed a current density above 0.5 V versus RHE. The reduction peak current density of PdO is -9.08 A g^{-1} in ~ 0.67 V versus RHE for PdMn(50:50)/C-ITO electrocatalyst, which is significantly larger than other electrocatalysts. This indicates the highest electrocatalytic activity of PdMn(50:50)/C-ITO electrocatalyst in the present work.

PdMn(50:50)/C-ITO electrocatalyst favors the methane oxidation for other products, such as CH_3OH, CH_2O_2, and CO_2, when compared to Pd/C-ITO and other electrocatalysts synthesized [36]. The increase in current density is possibly

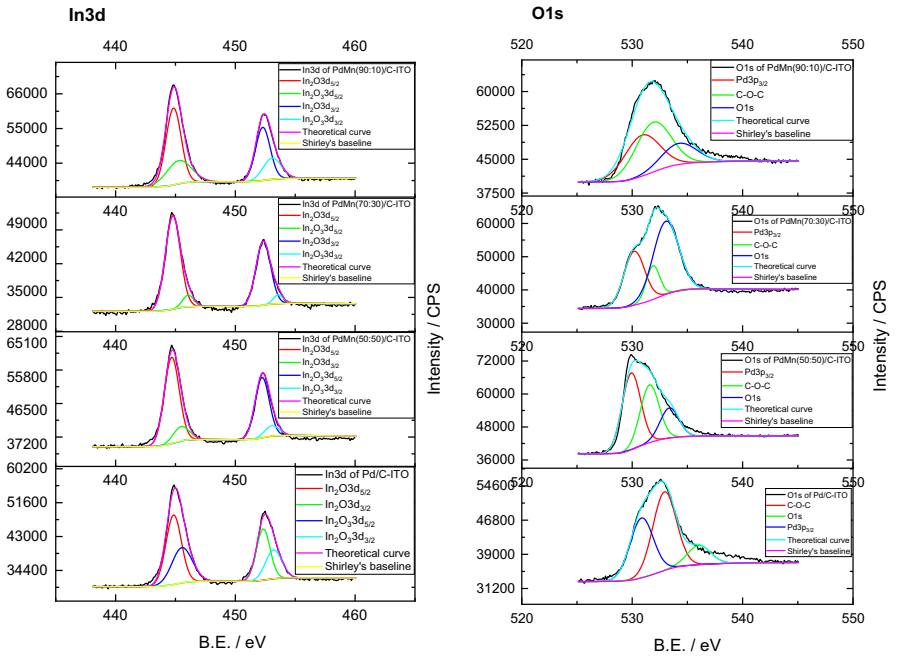

Fig. 4 XPS spectra of In3d and O1s of Pd/C-ITO, PdMn(90:10)/C-ITO, PdMn(70:30)/C-ITO and PdMn(50:50)/C-ITO electrocatalysts

attributed to the unique structure and electron transfer promotion properties of Mn at the electrode surface [47].

For all, binary electrocatalysts were also observed clear shifts of the peak positions to more negative potentials (0.47 V vs. RHE) in the hydrogen adsorption–desorption region when compared to Pd/C-ITO (0.54 V vs. RHE) cyclic voltammograms after methane adsorption (Fig. 6). These results agree partly in the work of Nandenha et al. [36]. However, this negative shift is an indication of the electronic modification of Pd atoms by the neighboring Mn atoms, MnO or In_2O_3 of ITO used as support [18, 36, 48]. This disagrees with the XRD results described above.

The oxygen reduction reaction (ORR) performance of the Pd/C-ITO, Mn/C-ITO and PdMn/C-ITO electrocatalysts synthesized was investigated using rotating ring-disk electrode (RRDE) technique [34, 46]. Figure 7 shows the linear sweep voltammetry (LSV) curve of all electrocatalysts recorded at a scan rate of 10 mV s^{-1} at 900 ppm rotational speed in oxygen purged 0.5 $HClO_4$ electrolyte and in ($O_2 + CH_4$ gases) purged in 0.5 mol L^{-1} $HClO_4$ electrolyte at room temperature.

The LSVs overlap completely in the activation and mixed control regions, but the limiting current for Pd/C-ITO, PdMn(90:10)/C-ITO and PdMn(50:50)/C-ITO electrocatalysts were even higher after the stability test (Fig. 7b_1, b_3, b_5) [49]. Clearly, these results indicate that Pd/C-ITO and PdMn(90:10)/C-ITO were more promising electrocatalysts for CH_3OH production in situ (Fig. 7b_1, b_3). It also shifts the CH_3OH formation to low potentials, facilitating the interaction of oxygen and CH_4

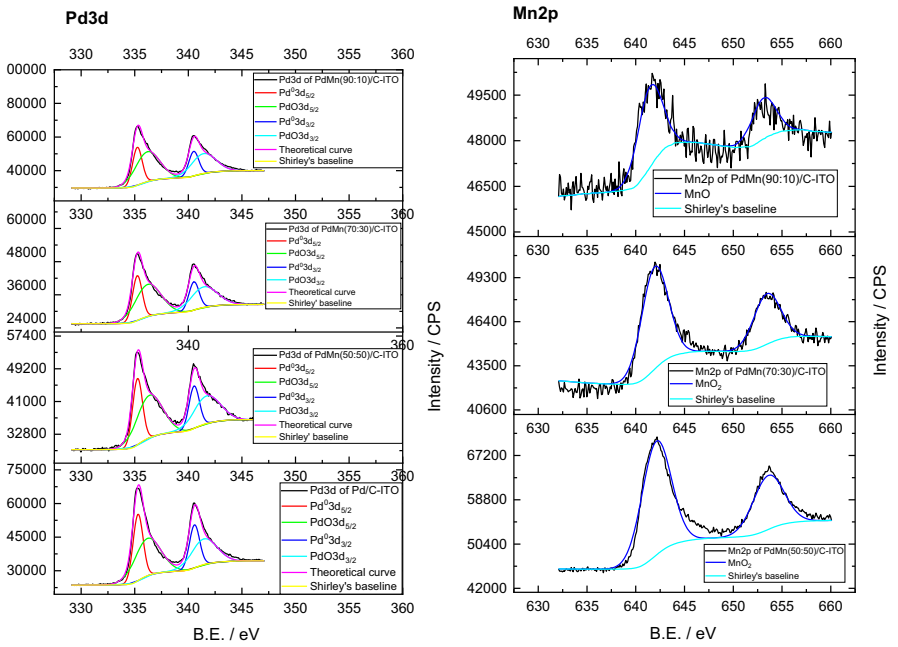

Fig. 5 XPS spectra of Pd3d and Mn2p of Pd/C-ITO, PdMn(90:10)/C-ITO, PdMn(70:30)/C-ITO and PdMn(50:50)/C-ITO electrocatalysts

gases with the Pd surface, hence increasing the activity of the electrocatalysts for the ORR in the CH_4 presence [46]. Pd/C-ITO, PdMn(90:10)/C-ITO and PdMn(50:50)/C-ITO shown an increasing lower on-set potential and higher current, whereas the Mn/C-ITO and PdMn(70:30)/C-ITO (Fig. 7b_2, b_4) followed oxygen purged in 0.5 $HClO_4$ electrolyte electro-reduction.

All potentials in this paper (Figs. 6, 7) are expressed with respect to the reversible hydrogen electrode (RHE) potential.

ATR-FTIR results

Figure 8 shows the absorbance spectra of an in situ electrochemical oxidation of CH_4 and CH_4 with O_2. It is possible to notice the presence of CH_4 in all potentials applied trough the degenerate deformation characteristic of the symmetric species in 1534 cm^{-1} and trough the degenerate stretching characteristic of the f_2 symmetry species [47]. Furthermore, all electrocatalysts exhibit the presence of Formic Acid trough the C–O stretching vibration in 1105 cm^{-1} [50] in the CH_4 and CH_4+O_2 experimental conditions.

Figure 8 also shows the presence of CH_3OH trough the CH_3 rock vibration mode [50], but only in the CH_4+O_2 experiment. O_2 plays an important role regarding CH_4 partial oxidation toward CH_3OH. We believe that O_2 molecules can activate the H_2O molecules leading to H_2O_2 which can react with CH_4 forming the CH_3OH species.

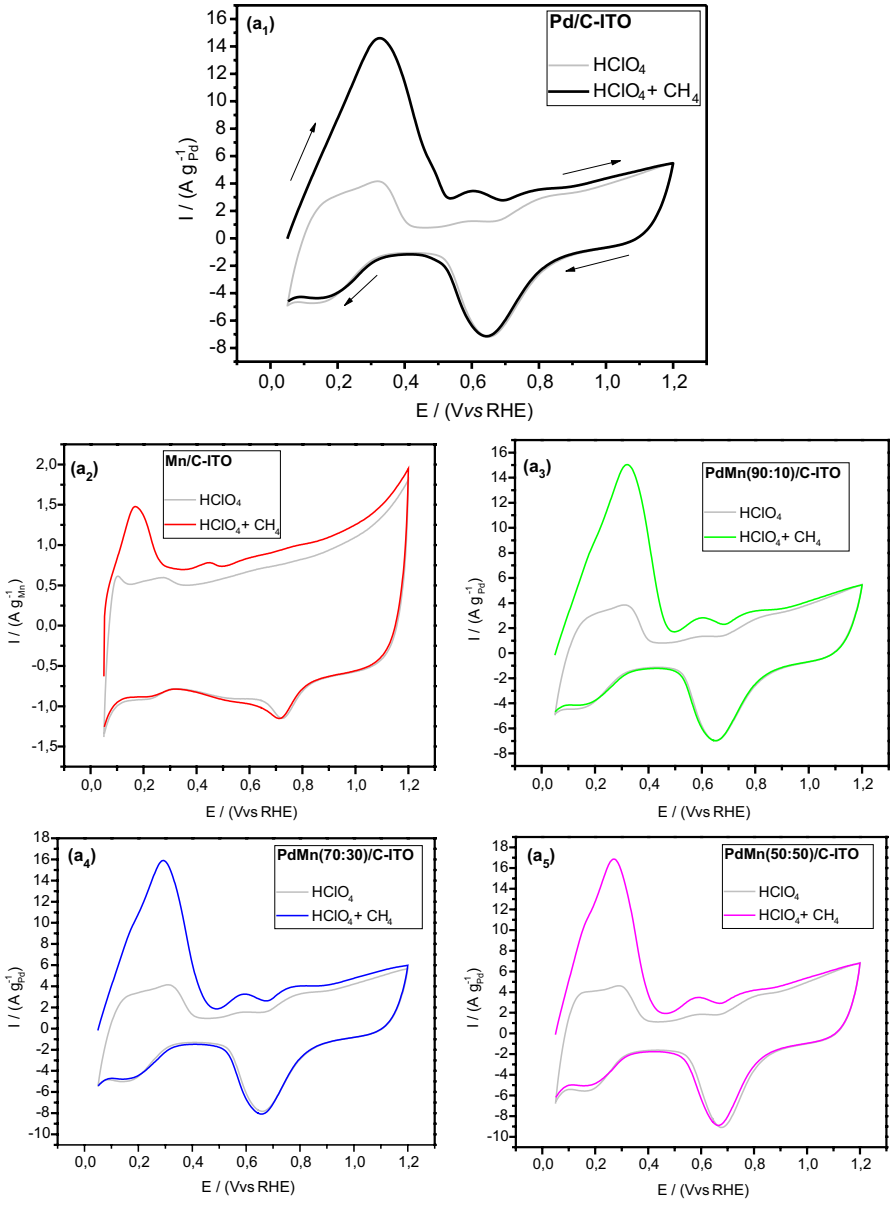

Fig. 6 Comparison of the voltammograms for $\mathbf{a_1}$ Pd/C-ITO, $\mathbf{a_2}$ Mn/C-ITO, $\mathbf{a_3}$ PdMn(90:10)/C-ITO, $\mathbf{a_4}$ PdMn(70:30)/C-ITO and $\mathbf{a_5}$ PdMn(50:50)/C-ITO: in a 0.5 mol L^{-1} $HClO_4$ electrolyte and 0.5 mol L^{-1} $HClO_4$ electrolyte + CH_4 gas, $\nu = 10$ mV s^{-1}; ambient temperature (300 K)

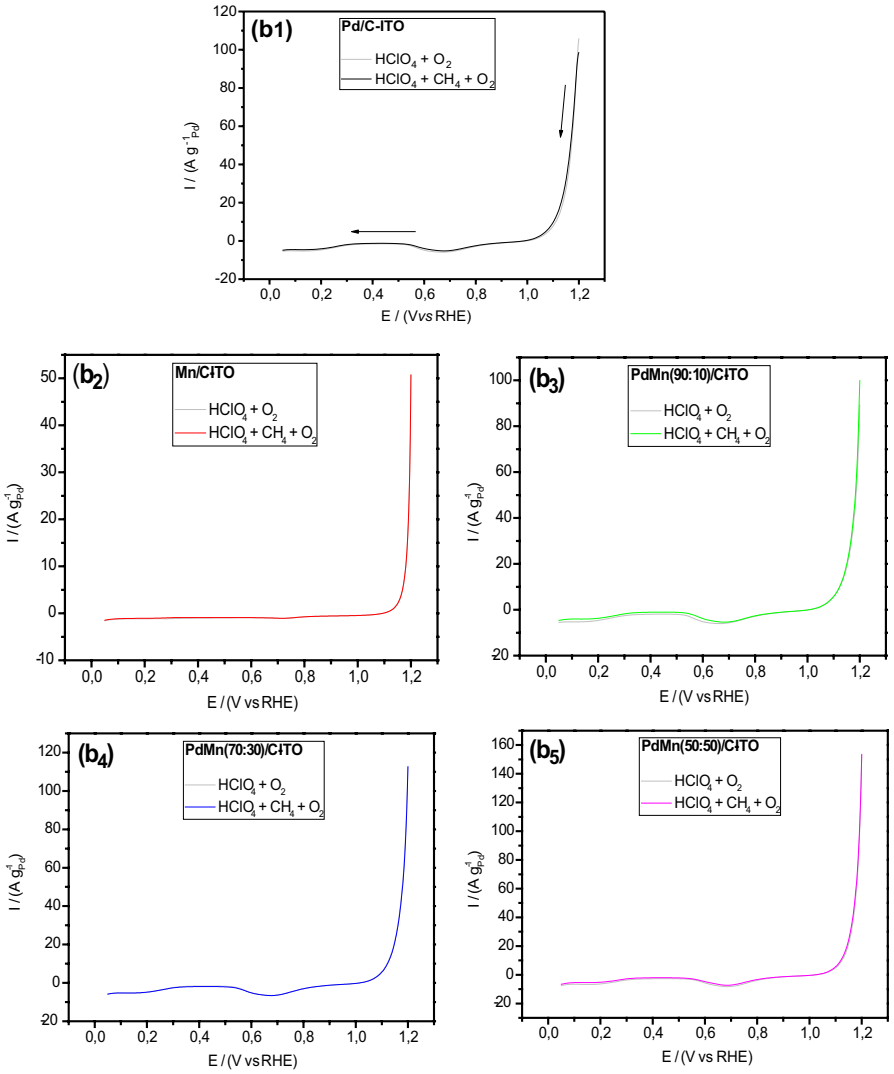

Fig. 7 Linear sweep voltammetry for $\mathbf{b_1}$ Pd/C-ITO, $\mathbf{b_2}$ Mn/C-ITO, $\mathbf{b_3}$ PdMn(90:10)/C-ITO, $\mathbf{b_4}$ PdMn(70:30)/C-ITO and $\mathbf{b_5}$ PdMn(50:50)/C-ITO in O_2 purged in 0.5 mol L^{-1} $HClO_4$ electrolyte and in (O_2+CH_4 gases) purged in 0.5 mol L^{-1} $HClO_4$ electrolyte at room temperature at a scan rate of 10 mV s^{-1} in anodic potential sweeps from 1.2 to 0.05 V versus RHE

DEFC experiments

The polarization and power density curves obtained in a single proton exchange membrane fuel cells using Pd/C-ITO, Mn/C-ITO, PdMn(90:10)/C-ITO, PdMn(70:30)/C-ITO and PdMn(50:50)/C-ITO, as anode electrodes are shown in Fig. 9. The open circuit voltage of the cell made with PdMn(70:30)/C-ITO

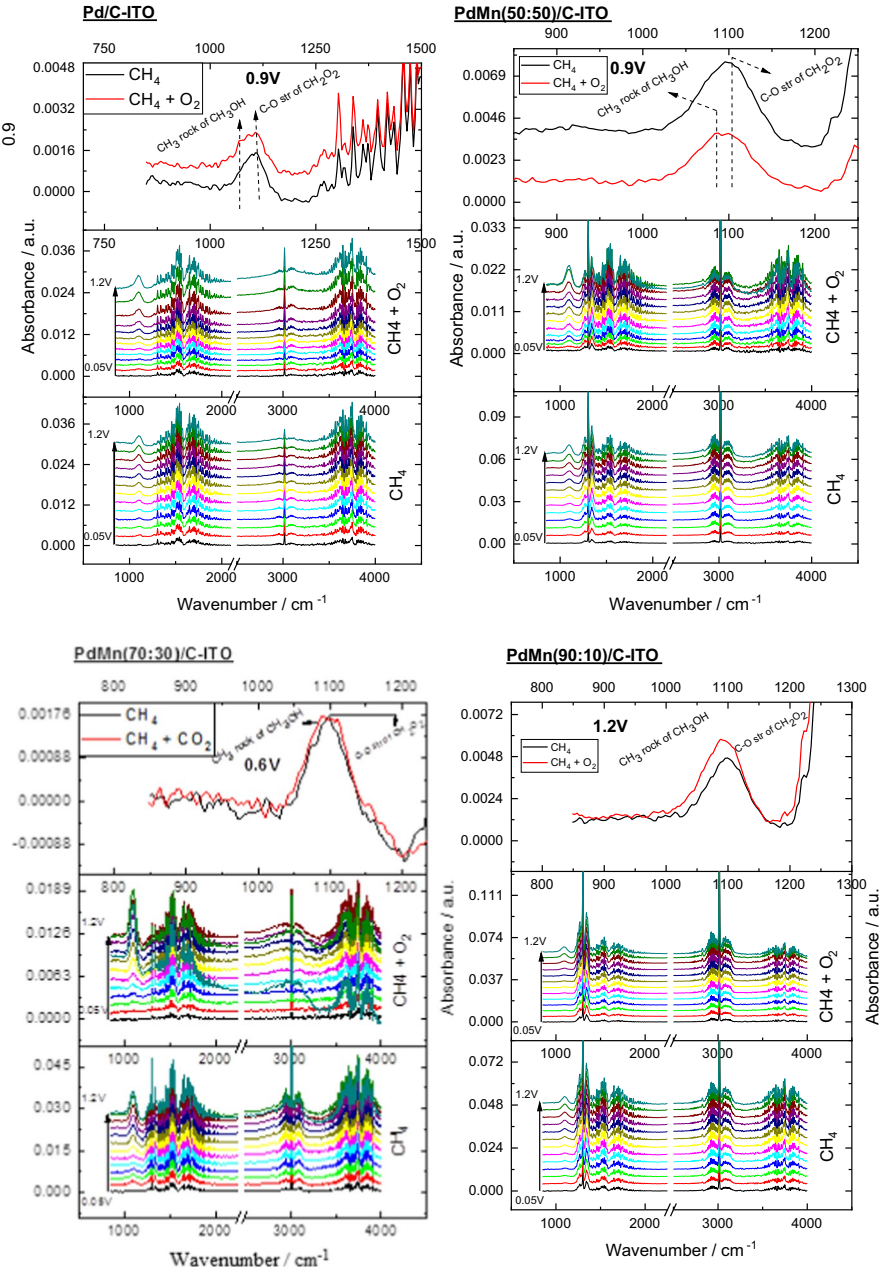

Fig. 8 ATR-FTIR spectra of Pd/C-ITO, PdMn(50:50)/C-ITO, PdMn(70:30)/C-ITO and PdMn(90:10)/C-ITO in 0.5 mol L^{-1} $HClO_4$ electrolyte + CH_4 gas flux in the presence of O_2 gas and 0.5 mol L^{-1} of $HClO_4$ electrolyte + CH_4 gas in the absence of O_2 gas

was ~ 1.10 V, some 0.48 V higher than that for Pd/C-ITO (~ 0.62 V) and also higher compared with PdMn(90:10)/C-ITO (~ 0.90 V), PdMn(50:50)/C-ITO (~ 0.84 V) and Mn/C-ITO (~ 0.67 V), respectively. This may be due to the fact that the high electrocatalyst dispersion helped to hinder the crossover of fuel from the anode to the cathode through the membrane pinholes [51].

PdMn(70:30)/C-ITO and PdMn(50:50)/C-ITO electrocatalysts indicated the highest value of maximum power density (4.9 mW cm^{-2} in 7.6 mA cm^{-2} and 3.6 mW cm^{-2} in 7.6 mA cm^{-2}), respectively, while Pd/C-ITO and Mn/C-ITO indicated value of similar power density (2.4 mW cm^{-2} in 6.7 mA cm^{-2} and 2.4 mW cm^{-2} in 5.7 mA cm^{-2}), respectively. The experiments at 80 °C showed that the addition of 30–50% Mn into Pd/C-ITO electrocatalyst promote methane activation. PdMn(70:30)/C-ITO showed superior performance for methane oxidation (4.9 mW cm^{-2} in 7.6 mA cm^{-2}) compared with others experiments at 80 °C, showing that the addition of 30% Mn into Pd/C-ITO electrocatalyst favor the methane electrooxidation. So, Pd/C-ITO indicated a decrease in kinetics reaction. The highest electrocatalytic activity of PdMn(70:30)/C-ITO and PdMn(50:50)/C-ITO prepared by borohydride reduction process could be attributed to the synergy between the constituents of the electrocatalyst (metallic Pd and Mn or In_2O, In_2O_3 and $In_2O_3{\cdot}SnO_2$). Thus, the presence of $In_2O_3{\cdot}SnO_2$ (ITO) could enhance the formation of chemisorbed oxygenated species which promotes the adsorbed carbon monoxide oxidation and/or adsorbed intermediates species, such as CO_{ads} and CH_3 on the surface of Pd. The enhancement of methane activation on PdMn/C-ITO could be caused by the changed reaction pathway due to ensemble effect or by the effective removal of CO_{ads} formed in the dehydration path resulted from the electronic effect of Mn donating electrons to the d-band of Pd [35, 52].

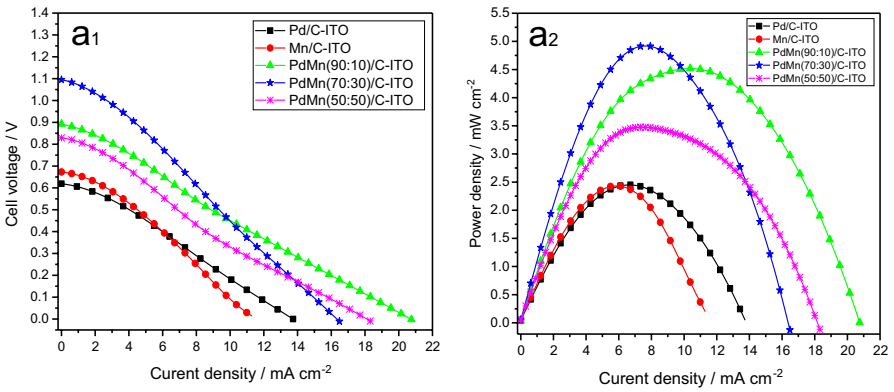

Fig. 9 $\mathbf{a_1}$ Polarization and $\mathbf{a_2}$ power density curves of a direct methane proton exchange membrane fuel cells (DMPEMFC) of 5 cm^2 at 80 °C using 150 mL min^{-1} methane flux

Conclusions

The method utilized in this work was an efficient methodology to produce PdMn/C-ITO for methane oxidation because ICP-MS and EDS results showed that the amount of Pd and Mn in the synthesized electrocatalysts is close to that expected.

The diffractograms of PdMn/C-ITO electrocatalysts showed four peaks at which are associated with crystal planes corresponding to the face-centered cubic structure (fcc), others peaks associated with the presence of a bixbyite In_2O_3 cubic structure, while for Mn/C-ITO and PdMn/C-ITO electrocatalysts no peaks relative to Mn or its oxides appeared, nevertheless, the presence of these peaks cannot be dismissed or its oxides can be present in very small amount or even in an amorphous form.

XPS results showed the presence of palladium and manganese oxides, in metallic palladium. For all the prepared electrocatalysts, it was observed in the anodic scan an increase in current in the hydrogen desorption region that correspond to hydrogen adsorption of methane. However, in the anodic scan, it was also observed a process of oxidation that could be attributed to formation of methanol and formic acidic observed by ATR-FTIR experiments.

The experiments at 80 °C in DMPEMFC showed that the addition of Mn to the Pd/C electrocatalyst promotes the methane activation by the bifunctional mechanism.

However, new studies are yet necessary to investigate the mechanisms of methane activation in alkaline electrolytes using PdMn/C-ITO.

Acknowledgements The authors thank the FAPESP (2014/09087-4, 2014/50279-4, 2017/11937-4, 2017/21846-6, 2017/10118-0 and 2017/22976-0), CINE-SHELL (ANP)/FAPESP Grants (2017/11937-4) and CNPq (300816/2016-2, 429727/2018-6 and 429727/2018-6) for the financial support.

References

1. W. Liemberger, M. Groß, M. Miltner, M. Harasek, J. Clean. Prod. **167**, 896 (2017)
2. A.W. Petrov, D. Ferri, F. Krumeich, M. Nachtegaal, J.A. van Bokhoven, O. Kröcher, Nat. Commun. **9**, 2545 (2018)
3. S. Xie, S. Lin, Q. Zhang, Z. Tian, Y. Wang, J. Energy Chem. **27**, 1629 (2018)
4. P. Schwach, X. Pan, X. Bao, Chem. Rev. **117**, 8497 (2017)
5. J. Lin, X. Wang, Sci. China Mater. **61**(5), 758 (2018)
6. M. Ravi, M. Ranocchiari, J.A. van Bokhoven, Angew. Chem. Int. Ed. **56**, 16464 (2017)
7. L. Arnarson, P.S. Schmidt, M. Pandey, A. Bagger, K.S. Thygesen, I.E.L. Stephens, J. Rossmeisl, Phys. Chem. Chem. Phys. **20**, 11152 (2018)
8. S. Specchia, F. Conti, V. Specchia, Ind. Eng. Chem. Res. **49**, 11101 (2010)
9. P. Gélin, M. Primet, Appl. Catal. B **39**, 1 (2002)
10. J. Nandenha, E.H. Fontes, R.M. Piasentin, F.C. Fonseca, A.O. Neto, J. Fuel Chem. Technol. **46**(9), 1137 (2018)
11. F. Hahn, C.A. Melendres, Electrochim. Acta **46**(23), 3525 (2001)
12. B. Suleiman, A.S. Abdulkareem, U. Musa, I.A. Mohammed, M.A. Olutoye, Y.I. Abdullahi, Energy Convers. Manag. **117**, 228 (2016)
13. X. Zhang, G. Juncheng, C. Jincan, Energy **35**, 5294 (2010)
14. K. Persson, K. Jansson, S.G. Järås, J. Catal. **245**, 401 (2007)
15. R. Abbasi, G. Huang, G.M. Istratescu, L. Wu, R.E. Hayes, Can. J. Chem. Eng. **93**, 1474 (2015)

16. J.J. Willis, E.D. Goodman, L. Wu, A.R. Riscoe, P. Martins, C.J. Tassone, M. Cargnello, J. Am. Chem. Soc. **139**, 11989 (2017)
17. H. Qiugu, J. Jinmei, Z. Qiao, Y. Xikun, L. Yan, M. Qi, Z. Yingjie, X. Mingli, Ionics. 26, 2421–2433 (2020).
18. M. Md. Abdul, J. Ji-Hoon, K. Young-Uk, J. Power Sources **262**, 356 (2014)
19. A. Mohammad Shamsuddin, P. Dongchul, J. Seungwon, J. Power Sources **308**, 180 (2016)
20. O. Lori, L. Elbaz, Catalysts **5**, 1445 (2015)
21. C.A. Ottoni, R.R. de Souza, S.G. da Silva, E.V. Spinacé, R.F.B. de Souza, A.O. Neto, Electroanalysis **29**, 960 (2017)
22. L. Shan-Shan, H. Yuan-Yuan, F. Jiu-Ju, L. Zhang-Ying, C. Jian-Rong, W. Ai-Jun, Int. J. Hydrog. Energy **39**, 3730 (2014)
23. H. Chen, J. Duan, X. Zhang, Y. Zhang, C. Guo, L. Nie, X. Liu, Mater. Lett. **126**, 9 (2014)
24. D. Schonvogel, J. Hulstede, P. Wagner, A. Dyck, C. Agert, M. Wark, J. Electrochem. Soc. **165**, F3373–F3382 (2018)
25. S.-Y. Huang, P. Ganesan, S. Park, B.N. Popov, J. Am. Chem. Soc. **131**, 13898 (2009)
26. Y. Liu, W.E. Mustain, Electrochim. Acta **115**, 116 (2014)
27. Y. Liu, W.E. Mustain, J. Am. Chem. Soc. **135**, 530 (2013)
28. K. Sasaki, L. Zhang, R.R. Adzic, Phys. Chem. Chem. Phys. **10**, 159 (2008)
29. C.V. Pereira, E.H. Fontes, J. Nandenha, M.H.M.T. Assumpção, A.O. Neto, Int. J. Electrochem. Sci. **13**, 10587 (2018)
30. V.F. de Camargo, E.H. Fontes, J. Nandenha, R.F.B. de Souza, A.O. Neto, Res. Chem. Intermed. **46**, 1555 (2020)
31. M. Brandalise, M.M. Tusi, R.M. Piasentin, M.C. dos Santos, E.V. Spinacé, A.O. Neto, Int. J. Electrochem. Sci. **7**, 9609 (2012)
32. M.C.L. Santos, J. Nandenha, J.M.S. Ayoub, M.H.M.T. Assumpção, A.O. Neto, J. Fuel Chem. Technol. **46**(12), 1462 (2018)
33. E.V. Spinacé, R.R. Dias, M. Brandalise, M. Linardi, A.O. Neto, Ionics **16**, 91 (2010)
34. F.M. Souza, J. Nandenha, B.L. Batista, V.H.A. Oliveira, V.S. Pinheiro, L.S. Parreira, A.O. Neto, M.C. Santos, Int. J. Hydrog. Energy **43**, 4505 (2018)
35. J. Nandenha, R.F.B. de Souza, M.H.M.T. Assumpção, E.V. Spinacé, A.O. Neto, Ionics **19**, 1207 (2013)
36. J. Nandenha, I.H.F. Nagahama, J.Y. Yamashita, E.H. Fontes, J.M.S. Ayoub, R.F.B. de Souza, F.C. Fonseca, A.O. Neto, Int. J. Electrochem. Sci. **14**, 10819 (2019)
37. T. Mittermeier, A. Weiß, H.A. Gasteiger, F. Hasché, J. Electrochem. Soc. **164**(12), F1081–F1089 (2017)
38. E.H. Fontes, C.E.D. Ramos, J. Nandenha, R.M. Piasentin, A.O. Neto, R. Landers, Int. J. Hydrog. Energy **44**, 937 (2019)
39. L. Feng, S. Yao, X. Zhao, L. Yan, C. Liu, W. Xing, J. Power Sources **197**, 38 (2012)
40. J. Nandenha, R.F.B. de Souza, M.H.M.T. Assumpção, E.V. Spinacé, A.O. Neto, Int. J. Electrochem. Sci. **8**, 9171 (2013)
41. L.L. Carvalho, A. Auro, A.A. Tanaka, F. Colmati, J. Solid State Electrochem. **22**, 1471 (2018)
42. C.A. Ottoni, C.E.D. Ramos, R.F.B. de Souza, S.G. da Silva, E.V. Spinacé, A.O. Neto, Int. J. Electrochem. Sci. **13**, 1893 (2018)
43. W.J. Zhou, S.Q. Song, W.Z. Li, Z.H. Zhou, G.Q. Sun, Q. Xin, S. Douvartzides, P. Tsiakaras, J. Power Sources **140**, 50 (2005)
44. J.F. Moulder, J. Chasatin, *Handbook of X-ray Photoelectron Spectroscopy: A Reference Book of Standard Spectra for Identification and Interpretation of XPS Data* (Perkin-Elmer Corporation Physical Electronics Division, Eden Prairie, 1992)
45. C. Lamy, B. Guenot, M. Cretin, G. Pourcelly, ECS Trans. **66**(29), 1 (2015)
46. Y. Zhang, L. Zhang, S. Shuang, F. Feng, J. Qiao, Y. Guo, M.M.F. Choi, C. Dong, Anal. Lett. **43**, 1055 (2010)
47. J. Qiao, S. Tang, Y. Tian, S. Shuang, C. Dong, M.M.F. Choi, Sens. Actuators B **138**, 402 (2009)
48. X. Zhang, H. Fan, J. Zheng, S. Duan, Y. Huang, Y. Cui, R. Wang, Catal. Sci. Technol. **8**, 4757 (2018)
49. W.R.P. Barros, Q. Wei, G. Zhang, S. Sun, M.R.V. Lanza, A.C. Tavares, Electrochim. Acta **162**, 263 (2015)
50. T. Shimanouchi, Tables of Molecular Vibrational Frequencies. National Standard Reference Data System, v. 1. Secretary of Commerce on Behalf of the United States Government (1972)

51. S. Limpattayanate, M. Hunsom, Int. Sch. Sci. Res. Innov. **9**(5), 659 (2015)
52. Y.-J. Chiou, K.-Y. Chen, H.-M. Lin, W.-J. Liou, H.-W. Liou, S.-H. Wu, A. Mikolajczuk, M. Mazurkiewicz, A. Malolepszy, L. Stobinski, A. Borodzinski, P. Kedzierzawski, K. Kurzydlowski, S.-H. Chien, W.-C. Chen, Phys. Status Solidi A **208**(8), 1778 (2011)